JOURNAL OF SOLID STATE CHEMISTRY 114, 52–56 (1995)

Crystal-Field Effect on the Magnetic Susceptibility of Rare-Earth (Pr, Nd, Eu) Mixed Oxides

C. Cascales,*,[1] R. Sáez-Puche,† and P. Porcher‡

*Instituto de Ciencia de Materiales de Madrid, CSIC, Serrano 113, E-28006 Madrid, Spain; †Departamento de Química Inorgánica, Facultad de Ciencias Químicas de la Universidad Complutense de Madrid, E-28040 Madrid, Spain; and ‡Laboratoire de Chimie Métallurgique et de Spectroscopie des Terres Rares, UPR 209 CNRS. F-92195 Meudon, France

Received November 17, 1993; in revised form March 16, 1994; accepted March 18, 1994

The comparison between the experimental and calculated magnetic susceptibility of Pr^{3+}, Nd^{3+}, and Eu^{3+} compounds in a wide group of materials, scheelite-type $Na_5RE(MoO_4)_4$, S.G. $I4_1/a$ (No. 88), cubic $RE_3Sb_5O_{12}$, S.G. $I43m$ (No. 217), monoclinic $RE_2Te_4O_{11}$, S.G. $C2/c$ (No. 15), and hexagonal $RE_3WO_6Cl_3$, S.G. $P6_3/m$ (No. 176) is reported. Structural and optical studies have shown that in every case the rare earth occupies *one single* crystallographic position, whose point symmetries are going from a relatively high symmetry, S_4 for both $Na_5RE(MoO_4)_4$ and $RE_3Sb_5O_{12}$ compounds, to very low symmetries, C_s and C_1 for $RE_3WO_6Cl_3$ and $RE_2Te_4O_{11}$, respectively. The magnetic susceptibilities have been measured in the temperature range 4.2–300 K. The experimental spectroscopic data were analyzed in terms of crystal-field theory for the $4f^2$, $4f^3$, and $4f^6$ configurations of the triply ionized Pr, Nd, and Eu ions, and then, using the wavefunctions associated with each energy level obtained from these analysis, the corresponding magnetic susceptibilities and their evolution vs temperature were simulated according to the van Vleck formalism. Satisfactory correlations, especially for Nd and Eu compounds, were achieved between the experimental and calculated magnetic susceptibilities, even when the approximate D_{2d} (near S_4) and C_{2v} and/or C_s (close to C_1) potentials were considered. Their observed deviation from the Curie–Weiss behavior at low temperature, very well reproduced, reflects the splitting of the ground state associated with these cations under the influence of the crystal field and is not due to any sort of magnetic interaction between the magnetic ions.

INTRODUCTION

In our preliminary studies (1–8) of the optical properties of the Pr^{3+}, Nd^{3+}, and Eu^{3+} configurations in several pure and doped compounds, the observed high-quality electronic spectra were analyzed according to crystal-field (cf) theory, and the experimental energy level schemes agree very well with those simulated. The accurate description of the spectroscopic properties of these materials is then the first step in the calculation of magnetic properties, such as the effective moment or the paramagnetic susceptibility (in this case due exclusively to the RE ions) and its variation vs temperature. For f electrons, the application of the magnetic tensor $L + g_eS$ on the obtained wavefunction associated with a given energy level leads to a good simulation of the observed data.

In this paper, we report the calculation of the paramagnetic susceptibility as a function of temperature for $RE = Pr^{3+}$ and Nd^{3+} in $Na_5RE(MoO_4)_4$, having S_4 point symmetry for the rare earth, and $RE_3WO_6Cl_3$, with C_s point symmetry. The studied samples are, in all cases, pure compounds in relation to the magnetic ions. The comparison with the corresponding calculations for other rare-earth mixed oxides families previously reported (1, 4, 8) allows us to underscore that the paramagnetic susceptibility and its evolution with temperature is well reproduced in these compounds, whatever the crystal-field strength and number of parameters involved in the simulation.

EXPERIMENTAL DETAILS

The magnetic susceptibility measurements on Pr, Nd, and Eu compounds on each studied series were performed by the Faraday method in applied fields of 12 kG from liquid-helium temperature to 300 K, using a DMS8 susceptometer. The setup was calibrated with $HgCo(SCN)_4$ and $Gd_2(SO_4)_3 \cdot 8H_2O$ as standards. The diamagnetic corrections were calculated using the standard values (in -1×10^{-6} emu $\cdot$ mol^{-1}) of 5, 7, 13, 14, 16, 17, 20, and 26 for Na^+, Mo^{6+}, W^{6+}, Te^{4+}, O^{2-}, Sb^{3+}, RE^{3+} (Pr, Nd, Eu), and Cl^-, respectively (9). The susceptibilities were found to be independent of the magnetic field in the temperature range of the measurements.

SIMULATION OF THE ENERGY LEVEL SCHEMES

The central-field approximation considers separately the Hamiltonians corresponding to the free-ion and crys-

[1] To whom correspondence should be addressed.

0022-4596/95 $6.00

tal-field interactions. The Hamiltonian used in the present study can be written as

$$H = H_0 - \sum_{K=0}^{K=3} E^K(nf, nf)e_K + \zeta_{4f}A_{SO} + \alpha L(L+1) + \beta G(G_2) + \gamma G(R_7) + \sum_{\lambda=2,\lambda\neq5}^{\lambda=8} T^\lambda t_\lambda,$$

where E^k and ζ_{4f} are the Racah parameters and the spin–orbit coupling constant, and e_k and A_{SO} represent the angular parts of the electrostatic repulsion and spin–orbit coupling, respectively. For the configurations of two or more equivalent electrons, the two-body interactions are considered with the Tree parameters α, β, and γ associated with the Casimir operators $G(G_2)$ and $G(R_7)$. For configurations having more than two electrons, nonnegligible three-body interactions can also be introduced (T^λ parameters). We do not consider here the spin–spin, spin–other-orbit, and other relativistic interactions of minor importance which could be simulated through the P^k ($k = 2, 4, 6$) and M_k ($k = 0, 2, 4$) integrals. In the present case, seven free-ion parameters can describe adequately the $4f^2$ configuration of Pr^{3+}. Since the $^1S_0$ level is only observed by means of two-photon spectroscopy, the γ parameter was fixed to a standard value. For the $4f^3$ and $4f^6$ configurations, the T^λ parameters are introduced. For the same reasons as for Pr^{3+}, some parameters (γ, T^2, and T^8) were fixed to values used in earlier studies (10, 11) for the $4f^3$ and $4f^6$ configurations.

The crystal-field calculations are usually carried out within the single-particle crystal-field theory. Following Wybourne's (12) formalism, the crystal-field Hamiltonian is expressed as a sum of products of spherical harmonics and crystal-field parameters:

$$H_{cf} = \sum_{k,q} (B_q^k[C_q^k + (-1)^q C_{-q}^k] + iS_q^k[C_q^k - (-1)^q C_{-q}^k]).$$

The number of nonzero B_q^k and S_q^k phenomenological crystal-field parameters (cfp's) depends on the crystallographic point-site symmetry of the lanthanide ion. For example, on the rare-earth tellurium oxides, the lanthanide ion occupies a crystallographic position with the very low C_1 point symmetry. The serial expansion of the cf potential keeps nonzero all of the 27 cf parameters, which constitutes nonrealistic conditions of simulation. Instead of C_1, the approximate C_s (or C_2 as well) point symmetry was used for the simulation, involving 14 nonzero cfp's, including five imaginary S_q^k. Moreover, if the imaginary part of the cfp's is cancelled, the symmetry increases up to C_{2v}, with only nine cfp's. The same situation corresponds to the symmetry of the $RE_3WO_6Cl_3$ materials. The approximated D_{2d} potential has been used for calculations in $RE_3Sb_5O_{12}$ compounds, involving five real B_q^k cfp's. The true symmetry S_4 was considered for $Na_5RE(MoO_4)_4$, including five real B_q^k and one additional imaginary S_q^k parameters.

The procedure to obtain the cfp's could be hardly facilitated if the cfp starting values had been estimated by a calculation from atomic positions. The most simplified model considers the effect of the electrostatic point charges localized at the crystallographic sites of the atoms on the network. We carried out calculations considering effective charges for the ions. Unfortunately, in some cases, these cfp's are too far from the experimental results. Finally, the best way is to consider the cfp's as phenomenological parameters to be derived from spectroscopic data.

The $4f^6$ configuration of Eu^{3+} is a convenient situation for starting the crystal-field calculations. In fact, the ground ^7F septet is well isolated from the rest of the configuration (the energy gap between $^7F_6$ and $^5D_0$ is $\approx$12,000 cm^{-1}); the crystal-field operator allows only the mixing of levels of the same multiplicity, and this is the only term with this multiplicity. Then, it is possible to calculate accurately the crystal-field effect by considering only the strongly reduced $^7F_{JM}$ basis, i.e., 49 $|SLJM_J\rangle$ states. In addition, the cfp's should vary smoothly in an isostructural series.

The energy level schemes are reproduced by diagonalizing the Hamiltonian matrix for each configuration. The simulations have been performed using the Fortran routines REEL and IMAGE (13).

MAGNETIC SUSCEPTIBILITY AND THE CRYSTAL-FIELD LEVELS

For rare-earth compounds the difference between experimental paramagnetic susceptibility and the Curie–Weiss law in the low-temperature range is generally due to crystal-field effects. The determination of consistent sets of eigenfunctions and eigenvalues from diagonalization of the above-mentioned crystal-field Hamiltonian permits the calculation of the magnetic susceptibility and effective magnetic moments of the rare earths. This is done using the van Vleck formula, the result of a perturbation created by an external applied magnetic field,

$$\chi(i) = N\beta^2 \sum_a \left[\frac{\langle\Phi_a|H|\Phi_a\rangle^2}{kT} - 2\sum_b \frac{\langle\Phi_a|H|\Phi_a\rangle\langle\Phi_a|H|\Phi_b\rangle}{E_a - E_b} \right] B_a,$$

in which N is Avogadro's number, β is the Bohr magneton, k is the Boltzmann constant, E and ϕ are the nonperturbed eigenvalues and wavefunctions, respectively, de-

scribed on the $|SLJM_J\rangle$ basis, and H is the magnetic dipole operator $L + g_e S$, represented by a first-rank tensor having three components which characterize the magnetic anisotropy. The different values of the tensor components (or combinations of them) destroy the isotropy observed for the free ion or even for an ion in a cubic symmetry. The anisotropic components are denoted $\chi_\perp$ (component ± 1 of the tensor) and $\chi_\parallel$ (component 0 of the tensor). For polycrystalline samples, the mean observed paramagnetic susceptibility is $\chi_{av} = (2\chi_\perp + \chi_\parallel)/3$. The sum runs over all thermally populated levels, according to the Boltzmann population, $B_a = \exp(-E_a^{(0)}/kT)/\Sigma_a \exp(-E_a^{(0)}/kT)$. In that expression, the matrix elements are calculated using the Racah algebra rules.

Except for Eu^{3+}, the diagonal part involving $E_i^{(1)}$ is the most important contribution to the paramagnetic susceptibility. In fact, it corresponds to the quantum expression of the Curie–Weiss law. The off-diagonal term in the formula, a result of the second-order perturbation, usually has small importance, with the exception of ground states with $J = 0$. The sum runs over all other states ($b \neq a$).

In rare-earth $4f^n$ configurations, the calculation of the paramagnetic susceptibility agrees fairly closely with experiment, especially for Nd compounds (14, 15). The high degeneracy of the $4f^6$ configuration makes the simulation more difficult for the Eu^{3+} compounds. The complete cf calculation would imply for a low symmetry (as is found for $RE_3WO_6Cl_3$ and $RE_2Te_4O_{11}$) to diagonalize a 3003-dimensioned matrix, which is not very feasible. For the C_{2v} symmetry, the problem is reduced to two submatrices whose size is approximately 1500. For the D_{2d} (or S_4) symmetry, it is reduced to four submatrices of about 750. Otherwise, Eu^{3+} presents an unique behavior: due to the nonmagnetic $^7F_0$ ground level, the diagonal part is cancelled at low temperatures when the next higher state $^7F_1$ is not populated, with only the second-order element in the above expression, $E^{(2)}_{^7F_0}$, nonvanishing. Then the nondiagonal interaction is the only one responsible for the paramagnetic susceptibility which is independent of the temperature, yielding a plateau in the χ–T plot. This indicates the sensitivity of the paramagnetic susceptibility to the value of this element, which, on the other hand, is strongly dependent on the cf strength. Anyway, very good correlations between the observed and simulated χ–T plots are obtained, (16, 17), the calculation showing plateaus at low temperature that agree very well with the experimental data.

RESULTS AND DISCUSSION

The phenomenological sets of free-ion and the crystal-field parameters have been collected elsewhere (1–8).

The comparison between the experimental and calculated average value of the temperature dependence of the reciprocal molar magnetic susceptibilities is plotted in Figs. 1–4. Symbols are used for experimental data, and solid lines for simulated curves from refined optical parameters.

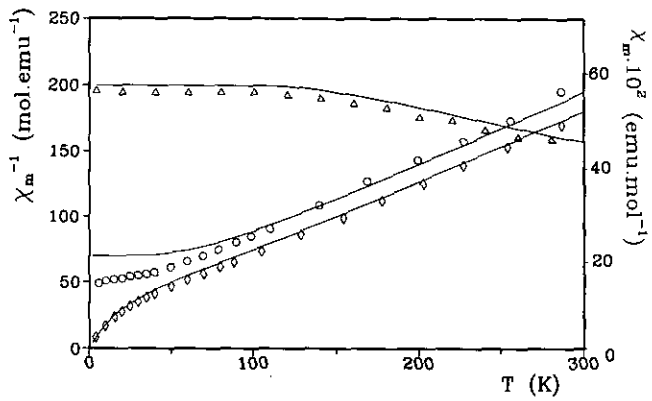

FIG. 1. Temperature variation of the magnetic susceptibility (Eu^{3+} compound) and reciprocal magnetic susceptibility (Pr^{3+}, Nd^{3+} compounds) in the $Na_5RE(MoO_4)_4$ series. Symbols (○, Pr; ◇, Nd; △, Eu) correspond to the experimental data and solid lines are the calculated average magnetic susceptibilities. (For the $Na_5Eu(MoO_4)_4$ the experimental measured susceptibility and the spectroscopic data have been taken from Ref. (24).)

The deviations from Curie–Weiss behavior, evident in the figures, at low temperature, reflects the splitting of the ground state associated with these cations under the influence of the crystal field.

Among all the Pr compounds, only $Pr_3Sb_5O_{12}$ exhibits a paramagnetic susceptibility curve perfectly simulated, as is the case for Nd and Eu compounds. For the other Pr compounds, both the experimental and the calculated curves of the reciprocal susceptibility bend upward to

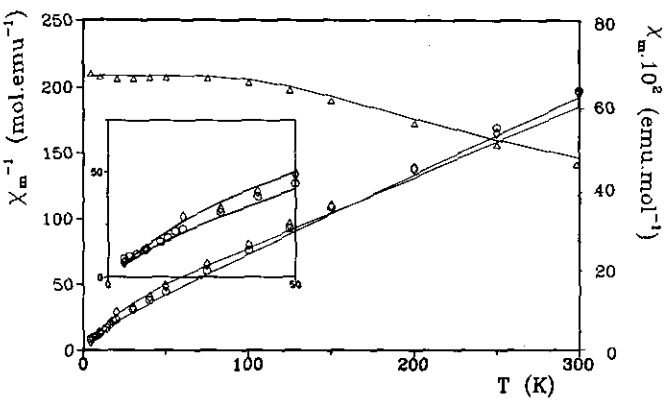

FIG. 2. Temperature variation of the magnetic susceptibility (Eu^{3+} compound) and reciprocal magnetic susceptibility (Pr^{3+}, Nd^{3+} compounds) in the $RE_3Sb_5O_{11}$ series. Symbols (○, Pr; ◇, Nd; △, Eu) correspond to the experimental data and solid lines are the calculated average magnetic susceptibilities.

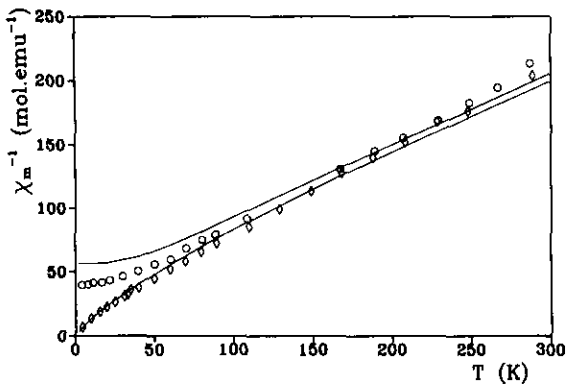

FIG. 3. Temperature variation of the reciprocal magnetic susceptibility for Pr^{3+} and Nd^{3+} compounds in the $RE_3WO_6Cl_3$ series. Symbols (○, Pr; ◇, Nd) correspond to the experimental data and solid lines are the calculated average magnetic reciprocal susceptibilities.

level off below ≈35–60 K. The materials show, above ≈150–200 K, experimental reciprocal susceptibilities larger than those calculated, but below these temperatures the situation is reversed. It is clear that the discrepancy has nothing to do with the simulation procedure or the approximate calculation induced by the symmetry lowering, because $PrVO_4$ and $Na_5Pr(MoO_4)_4$ do have higher point symmetries (D_{2d} and S_4) as well as $Pr_3Sb_5O_{12}$ (S_4) does. Also, an accidental lifting of the E irreducible representation of the ground state is excluded for $Pr_3WO_6Cl_3$ and $Pr_2Te_4O_{11}$ (low point symmetry). The same type of mismatch has been observed in previously reported data for $PrVO_4$ (18) and PrF_3 (19).

Three possible arguments can be proposed to explain this mismatch:

(i) The $4f^2$ configuration basis is not large enough to reproduce the Pr^{3+} properties. It has been shown elsewhere (20, 21) that the mixing with the first excited configuration $4f^15d^1$ through the odd parameters of the crystal-field expansion permits a good reproduction of $^1D_2$ splitting, which is not the case when the ground configuration is considered isolately. Consequently, the wavefunctions will be affected.

(ii) Possible couplings between the phonons of the system and electronic levels, i.e., the first excited $^3H_4$ crystal field level, as was suspected in Ref. (22). It is possible to reproduce correctly the paramagnetic susceptibility if this level is lowered by choosing an adequate cfp set. Naturally in that case the experimental energy level scheme is no longer reproduced.

(iii) The last and more simple explanation lies in the large anisotropy found for these compounds in the calculation of the paramagnetic susceptibility at low temperature, decreasing with increasing temperature (see, e.g., the data for $Pr_2Te_4O_{11}$, Table 2, Ref. (8)). It is thus possible that preferred orientations could exist for the magnetic susceptibility measurement of the polycrystalline powder. In a similar way, calculations of magnetic susceptibility from optical data on REF_3 matrices, RE = Pr^{3+} and Nd^{3+} (19), also show highly anisotropic behavior at low temperatures for the PrF_3 compound. The problem will be solved by measurements on single crystals. In fact, these anisotropic effects have been fully reproduced in some studies (23) on crystals of dilute alloys of Pr in Y and Lu.

The experimental and calculated curves for Nd materials agree well over the entire measured temperature range, especially at low temperature; the deviation from the Curie–Weiss law, as a consequence of the crystal-field splitting, is very well reproduced.

The magnetic susceptibility of Eu compounds increases with decreasing temperature down to about 70 K; below this temperature, it flattens out. At very low temperature, the increasing paramagnetic susceptibility is probably due to a small amount of divalent Eu impurity always presents in Eu mixed oxides. Its strong paramagnetic character, especially at low temperature ($\mu_{eff} \approx 7.94$ BM), permits us to estimate a concentration lower than 0.1%.

Although the crystal field is usually assumed to be temperature-independent, in fact the network parameters smoothly vary with the temperature. However, when there is no phase transition, and for the rare-earth compounds, these variations have a negligible effect upon the crystal field parameters. This means that the calculation of a broad range of the $\chi(T)$ function in terms of a single set of parameters is entirely acceptable.

For most of the transparent rare-earth compounds, the optically active $4f$ electrons are not—or not quite—active in the chemical bonding because of protection by an external electron sheet, and for the ion embedded in the crystalline matrix they practically maintain the same energy level

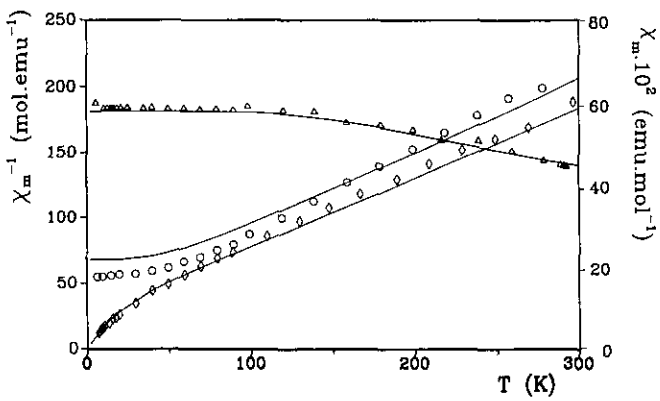

FIG. 4. Temperature variation of the magnetic susceptibility (Eu^{3+} compound) and reciprocal magnetic susceptibility (Pr^{3+}, Nd^{3+} compounds) in the $RE_2Te_4O_{11}$ series. Symbols (○, Pr; ◇, Nd; △, Eu) correspond to the experimental data and solid lines are the calculated average magnetic susceptibilities.

sequence as that of the free ion; as a first consequence, both magnetic moments will be closely related. Therefore these compounds do not undergo any magnetic exchange interactions. In this way, the good agreement found between experimental paramagnetic susceptibility measurements and our calculations using wavefunctions taking into account the crystal-field effect underscores that it is generally not necessary to introduce coupling or exchange interactions between rare-earth ions in covalent compounds. However, the mismatch observed for the praseodymium ion case suggests that the basis to be considered for the wavefunctions should include excited configurations, although these ions have mostly a "$4f$" character.

ACKNOWLEDGMENT

One of the authors (C.C.) thanks the Comisión Interministerial de Ciencia y Tecnología (CICYT) of the Spanish Educational Office for financial support.

REFERENCES

1. R. Sáez-Puche, E. Antic-Fidancev, M. Lemaitre-Blaise, P. Porcher, C. Cascales, C. M. Marcano, and I. Rasines, *J. Less-Common Met.* **148,** 369 (1989).
2. C. Cascales, E. Antic-Fidancev, M. Lemaitre-Blaise, and P. Porcher, *J. Solid State Chem.* **89,** 118 (1990).
3. C. Cascales, E. Antic-Fidancev, M. Lemaitre-Blaise, and P. Porcher, *Eur. J. Solid State Inorg. Chem.* **28,** 93 (1991).
4. E. Antic-Fidancev, C. Cascales, M. Lemaitre-Blaise, P. Porcher, R. Sáez-Puche, and I. Rasines, *Eur. J. Solid State Inorg. Chem.* **28,** 77 (1991).
5. C. Cascales, E. Antic-Fidancev, M. Lemaitre-Blaise, and P. Porcher, *An. Quim. (Spain)* **87,** 1005 (1991).
6. C. Cascales, E. Antic-Fidancev, M. Lemaitre-Blaise, and P. Porcher, *J. Phys.: Condens. Matter* **4,** 2721 (1992).
7. C. Cascales, E. Antic-Fidancev, M. Lemaitre-Blaise, and P. Porcher, *J. Alloys Comp.* **180,** 111 (1992).
8. C. Cascales, P. Porcher, and R. Sáez-Puche, *J. Phys. Chem. Solids* **54,** 1471 (1993).
9. L. N. Mulay, "Magnetic Susceptibility," p. 1782. Wiley, New York, 1963.
10. P. Caro, D. R. Svoronos, E. Antic-Fidancev, and M. Quarton, *J. Chem. Phys.* **66,** 5284 (1977).
11. A. A. S. DaGama, G. F. De Sa, P. Porcher, and P. Caro, *J. Chem. Phys.* **75,** 2583 (1981).
12. B. G. Wybourne, "Spectroscopic Properties of Rare Earths." Wiley, New York, 1965.
13. P. Porcher, Computer programs REEL and IMAGE for simulation of d^n and f^n configurations involving real and complex crystal field parameters. Unpublished, 1989.
14. P. Caro, J. Derouet, L. Beaury, G. Teste de Sagey, J. P. Chaminade, J. Aride, and M. Pouchard, *J. Chem. Phys.* **74,** 2698 (1981).
15. P. Caro, J. Derouet, L. Beaury, and E. Soulie, *J. Chem. Phys.* **70,** 2542 (1975).
16. C. K. Jayansankar, E. Antic-Fidancev, M. Lemaitre-Blaise, and P. Porcher, *Phys. Status Solidi B* **133,** 345 (1985).
17. P. Caro and P. Porcher, *J. Magn. Magn. Mater.* **58,** 61 (1986).
18. M. D. Guo, A. T. Aldred, and S. K. Chan, *J. Phys. Chem. Solids* **48,** 229 (1987).
19. C. Leycuras-Coulon, Ph.D. Thesis. Université de Paris-Sud, Orsay, 1984.
20. M. Faucher, D. Garcia, P. Caro, J. Derouet, and P. Porcher, *J. Phys. (Paris)* **50,** 219 (1989).
21. D. Garcia and M. Faucher, *J. Chem. Phys.* **90,** 5280 (1989).
22. O. K. Moune, P. Porcher, and P. Caro, *J. Solid State Chem.* **50,** 41 (1983).
23. P. Toubourg, R. Nevald, and T. Johansson, *Phys. Rev. B* **17,** 4454 (1987).
24. J. Huang, J. Loriers, P. Porcher, G. Teste de Sagey, P. Caro, and C. Levy-Clement, *J. Chem. Phys.* **80**(12), 6204 (1984).